THE JOURNAL OF BIOLOGICAL CHEMISTRY VOL. 287, NO. 9, pp. 6454–6468, February 24, 2012

Induction of COX-2 Enzyme and Down-regulation of COX-1 Expression by Lipopolysaccharide (LPS) Control Prostaglandin E_2 Production in Astrocytes*[S]

Received for publication, November 27, 2011 Published, JBC Papers in Press, January 4, 2012, DOI 10.1074/jbc.M111.327874

Miriam Font-Nieves[1], **M. Glòria Sans-Fons, Roser Gorina, Ester Bonfill-Teixidor, Angélica Salas-Pérdomo, Leonardo Márquez-Kisinousky, Tomàs Santalucia, and Anna M. Planas**[2]

From the Department of Brain Ischemia and Neurodegeneration, Institute for Biomedical Research of Barcelona, Consejo Superior de Investigaciones Científicas, Institut d'Investigacions Biomèdiques August Pi i Sunyer, 08036 Barcelona, Spain

Background: The relative contribution of COX-2 and COX-1 to prostanoid formation under neuroinflammation is complex.
Results: LPS induced COX-2 and mPGES1 but down-regulated COX-1 and TS in astroglia. These effects accounted for the high production of PGE_2.
Conclusion: PGE_2 after LPS results from the coordinated COX-2 up-regulation and COX-1 down-regulation in astrocytes.
Significance: Changes in COX-2 and COX-1 expression mediate astroglial PGE_2 generation in neuroinflammation.

Pathological conditions and pro-inflammatory stimuli in the brain induce cyclooxygenase-2 (COX-2), a key enzyme in arachidonic acid metabolism mediating the production of prostanoids that, among other actions, have strong vasoactive properties. Although low basal cerebral COX-2 expression has been reported, COX-2 is strongly induced by pro-inflammatory challenges, whereas COX-1 is constitutively expressed. However, the contribution of these enzymes in prostanoid formation varies depending on the stimuli and cell type. Astrocyte feet surround cerebral microvessels and release molecules that can trigger vascular responses. Here, we investigate the regulation of COX-2 induction and its role in prostanoid generation after a pro-inflammatory challenge with the bacterial lipopolysaccharide (LPS) in astroglia. Intracerebral administration of LPS in rodents induced strong COX-2 expression mainly in astroglia and microglia, whereas COX-1 expression was predominant in microglia and did not increase. In cultured astrocytes, LPS strongly induced COX-2 and microsomal prostaglandin-E_2 (PGE_2) synthase-1, mediated by the MyD88-dependent NFκB pathway and influenced by mitogen-activated protein kinase pathways. Studies in COX-deficient cells and using COX inhibitors demonstrated that COX-2 mediated the high production of PGE_2 and, to a lesser extent, other prostanoids after LPS. In contrast, LPS down-regulated COX-1 in an MyD88-dependent fashion, and COX-1 deficiency increased PGE_2 production after LPS. The results show that astrocytes respond to LPS by a COX-2-dependent production of prostanoids, mainly vasoactive PGE_2, and suggest that the coordinated down-regulation of COX-1 facilitates PGE_2 production after TLR-4 activation. These effects might induce cerebral blood flow responses to brain inflammation.

Cyclooxygenases (COX),[3] also known as prostaglandin G/H synthases, play a crucial role in inflammation and are targets of widely used nonsteroidal anti-inflammatory drugs. There are two main COX enzymes, COX-1 and COX-2, that participate in the metabolism of arachidonic acid generating the unstable product prostaglandin (PG) G_2 that is reduced to PGH_2. PGH_2 is the substrate of prostaglandin isomerases that give rise to a family of vasoactive compounds called prostanoids, including molecules such as prostaglandins, thromboxane, and prostacyclin. There is cellular specificity for the production of certain prostanoids, and they exert different actions depending on the type of molecule produced and on the specific receptors that become activated (1). Although COX-1 is constitutively expressed in most tissues, COX-2 is an inducible enzyme that responds to pro-inflammatory stimuli.

COX-2 is induced in brain cells under pathological conditions, but the role of the COX isoforms in brain diseases is not clearly established. *Cox-2*-deficient mice are protected against brain ischemia (2), and inhibition of COX-2 provides beneficial effects against ischemic damage and neuronal death (3–6), suggesting a detrimental effect of COX-2 in stroke. In contrast, in neurodegenerative diseases, COX-2 inhibitors are not protective in mouse models of Alzheimer disease (7) and did not show benefits in clinical trials in Alzheimer disease patients (8) or in patients with mild cognitive impairment (9). Furthermore, COX-2 inhibitors increase the risk of cardiovascular and cerebrovascular pathology (10), and *Cox-2*-deficient mice show exacerbated brain inflammation, leukocyte infiltration, and

* This work was supported in part by Spanish Ministry of Science and Innovation Grant SAF2008-04515 and by European Community FP7/2007-2013 Project, Agreement 201024.
[S] This article contains supplemental Figs. 1–4.
[1] Recipient of a Ph.D. fellowship from the Spanish Ministry of Science and Innovation.
[2] To whom correspondence should be addressed: Dept. of Brain Ischemia and Neurodegeneration, IIBB-CSIC, IDIBAPS, Rosselló 161, Planta 6, 08036 Barcelona, Spain. Tel.: 34-93-363-83-27; Fax: 34-93-363-83-01; E-mail: anna.planas@iibb.csic.es.

[3] The abbreviations used are: COX, cyclooxygenase; PG, prostaglandin; $cPLA_2$, cytosolic phospholipase A_2; CBF, cerebral blood flow; TxB_2, thromboxane B_2; TxA_2, thromboxane A_2; PDTC, pyrrolidinedithiocarbamate; TS, thromboxane synthase; GFAP, glial fibrillary acidic protein.

blood-brain barrier damage after exposure to the bacterial lipopolysaccharide (LPS) (11–15), suggesting some beneficial action of COX-2 in inflammation. Furthermore, COX-2 might contribute to neurovascular coupling because COX-2 inhibitors abrogate the increases in cerebral blood flow (CBF) induced by neuronal activation in rats (16). Exposure to LPS has been reported to induce vasodilation (17) and increase CBF (18) through a mechanism involving inducible NOS and the *NOX2* subunit of the superoxide-producing enzyme NADPH oxidase. Because LPS induces strong expression of COX-2 in the brain, it is feasible that vasoactive COX-2 products might also be involved in CBF regulation.

In this study we examined the effect of intracerebral administration of LPS on the cellular expression of COX-2 and found strong up-regulation in microglia and astrocytes. Because astrocytes are recognized as important players in CBF regulation under physiological and pathological conditions (19), we then investigated the prostanoids induced by LPS and the COX isoforms involved in prostanoid generation in purified astrocyte cultures. The results show that the LPS challenge strongly induced COX-2 in astrocytes through a MyD88/NFκB-dependent mechanism, show the crucial role of COX-2 in prostanoid production after LPS, and show that PGE_2 is the major product of arachidonic acid metabolism under these experimental conditions. Furthermore, we found that LPS down-regulates *Cox-1* gene expression and that *Cox-1*-deficient cells produce more PGE_2 than the WT, indicating some negative effect of COX-1 on the COX-2-dependent production of PGE_2 in astrocytes after LPS.

EXPERIMENTAL PROCEDURES

Animals—Animal work was authorized by the Ethical Committee of the University of Barcelona, and it was performed in agreement with the local regulations and in compliance with the Directives of the European Community. Four-month-old male Sprague-Dawley rats were obtained from Charles River (Lyon, France). MyD88 knock-out (KO) mice in a C57Bl/6 background were obtained from Oriental Bioservices, Inc. (Kyoto, Japan). MyD88 KO mice (−/−) were crossed with wild type (WT) (+/+) C57Bl/6 mice (Charles River), and a colony of MyD88 heterozygous mice (+/−) was kept in the animal house of the University of Barcelona School of Medicine. Each individual animal born from the heterozygous progenitors was genotyped, and the MyD88 KO and the MyD88 WT animals were selected for the studies described below. COX-1 and COX-2 heterozygous mice were from Taconics Inc. (Hudson, NY). COX-2 or COX-1 heterozygous females (+/−) were crossed with homozygous (−/−) males; all had a mixed B6;129P2 background. We genotyped each animal of the offspring, and the KO animals were selected for the studies, although the corresponding WT animals were used as controls.

Genotyping Protocols—Genotyping was carried out by doing PCR on DNA extracted from tail biopsies. The Extract-N-Amp Tissue PCR kit (Sigma) was used for the extraction of DNA and preparation of PCRs according to the manufacturer's instructions. For experiments with COX KO or WT cells, the following sets of primers (20) were used for PCR: Cox-1 KO forward, 5′-GCAGCCTCTGTTCCACATACAC-3′; Cox-1 WT forward, 5′-AGGAGATGGCTGCTGAGTTGG-3′; Cox-1 reverse (common), 5′-AATCTGACTTTCTGAGTTGCC-3′; Cox-2 KO forward, 5′-ACGCGTCACCTTAATATGCG-3′; Cox-2 WT forward, 5′-ACACCTTCAACATTGAAGACC-3′; Cox-2 reverse (common), 5′-ATCCCTTCACTAAATGCCCTC-3′. Amplicon sizes were as follow: Cox-1 WT, 601 bp; Cox-1 KO, 646 bp; Cox-2 WT, 725 bp; Cox-2 KO, 905 bp. The cycling parameters were 94 °C, 5 min for initial denaturation, followed by 34 cycles of denaturation at 94 °C for 30 s, primer annealing at 60 °C (Cox-1) or 57 °C (Cox-2) for 30 s, and extension at 72 °C for 1 min. The last cycle was followed by an additional extension step at 72 °C for 5 min. The supplemental material depicts an example of a genotyping reaction (supplemental Fig. 1). For experiments with MyD88 KO mice, the genotyping procedure has been reported previously (21).

LPS Administration to Rodents—Rats and mice were anesthetized with isofluorane and placed in a stereotaxic apparatus for injection of LPS or the vehicle (phosphate-buffered saline (PBS)) in the right striatum. For rats, LPS (5 μl of 1 μg/ml) or the same volume of vehicle was injected at the following coordinates according to the atlas of Paxinos and Watson (22) in relation to Bregma as follows: 0.5 mm antero-posterior, 3 mm lateral, and 5 mm ventral. For mice, LPS (0.7 μl of 1 μg/ml) or vehicle was injected at the following coordinates: 0.5 mm antero-posterior, 2 mm lateral, and 3 mm ventral. After 8 h, animals were anesthetized with isofluorane and perfused through the heart with saline to remove blood from the brain vessels, and brain tissue was obtained after dissection of the ipsilateral and contralateral striatum and was immediately frozen and kept at −80 °C until further use. A different set of animals was processed for immunohistochemistry.

Cell Cultures—Glial cell cultures enriched in astrocytes were prepared from the cerebral cortex of 1–2-day-old rats or mice as described previously (21, 23), with minor modifications. In brief, cells were maintained at 37 °C in a humidified atmosphere of 5% CO_2, 95% air in culture medium (DMEM (Invitrogen) for rat astrocytes, and DMEM/F-12 nutrient (1:1) (Invitrogen) for mouse astrocytes). Media were supplemented with 10% fetal bovine serum (FBS; Invitrogen) and 4 ml/liter of a mixture of penicillin/streptomycin 10,000 units, 10,000 μg/ml (Invitrogen). Cells were subcultured to obtain purified astroglia cultures, as follows. At confluence after 8–10 days *in vitro*, cells were treated with 4 μM antimitotic cytosine arabinoside (Sigma) for 5 days to eliminate dividing cells, *i.e.* mostly microglia and progenitors. Flasks were shaken overnight, and the remaining astrocyte adherent monolayer was detached with trypsin 0.0125%, 0.2 mM EDTA and seeded at 10×10^4 cells/ml with incubation medium (as above). Purified astrocytes were treated when cells reached confluence at 4 days after subculturing. FBS was reduced to 1% 16 h prior to treatments.

Rat astrocyte cultures contained only 2.01 ± 1.68% of contaminating microglia cells, as reported (21). Purified mouse astrocyte cultures also contained very little microglia, as estimated by immunofluorescence and by examining the expression of *CD11b* mRNA (see below for description of these methods). After immunofluorescence with an antibody against a microglial marker (Iba-1) and an antibody against glial fibrillary

acidic protein (GFAP) to label astrocytes (supplemental Fig. 2), we counted ($n = 24$ fields for two cultures, using ×20 magnification) the percentage of Iba-1 immunoreactive cells and estimated that the % of contaminating microglia in the astrocyte cultures was 0.77 ± 0.49%. Independently, we calculated the percentage of *CD11b* expression per culture by real time RT-PCR as a marker of microglia and used purified microglia cultures (obtained as reported previously (24)) as a reference for 100% *CD11b* expression. According to this procedure, *CD11b* expression (mean ± S.D., $n = 5$) in astroglia cultures was 1.41 ± 1.22%, supporting that contaminating microglia cells were very scarce in the purified astroglia cultures.

For experiments with MyD88 KO, Cox-1 KO, and Cox-2 KO cells, individual astrocyte cultures were obtained from each newborn animal and, after genotyping, the −/− (KO) and +/+ (WT) cultures were selected for use in further experiments. Experiments in KO and WT cells were carried out in parallel.

Drug Treatments—Cells were exposed to 10 ng/ml LPS (*Escherichia coli* 055:B5) (Sigma) for times ranging from 4 to 24 h. Cells were treated with the following mitogen-activated protein kinase (MAPK) inhibitors (Calbiochem): MAPK kinase (MEK) inhibitors 1,4-diamino-2,3-dicyano-1,4-bis(2-aminophenylthio)butadiene (U0126) (1–25 μM) and PD98059 (1–40 μM); p38 MAPK inhibitor *trans*-4-[4-(4-fluorophenyl)-5-(2-methoxy-4-pyrimidinyl)-1*H*-imidazol-1-yl]cyclohexanol (SB239063) (0.1–25 μM); and stress-activated SAPK/MAPK inhibitor anthra(1,9-*cd*)pyrazol-6(2*H*)-one (SP600125) (1–25 μM) that was dissolved in dimethyl sulfoxide (DMSO) (Sigma) and given 30 min prior to LPS. COX-2 inhibitor *N*-[cyclohexyloxy-4-nitrophenyl] methanesulfonamide (NS-398) was purchased from Tocris Bioscience (Ellisville, MO), dissolved in saline, pH 13, and used at 3 μM. COX-1 inhibitor 5-(4-chlorophenyl)-1-(4-methoxyphenyl)-3-trifluoromethylpyrazole (SC-560) was purchased from Calbiochem, dissolved in DMSO, and used at 10 nM. Treatment with COX inhibitors was carried within 30–60 min prior to LPS. The cytosolic phospholipase A_2 ($cPLA_2$) inhibitor arachidonyltrifluoromethyl ketone (Calbiochem) was dissolved in DMSO and used at 2 μM 30 min before LPS. For all drugs, the corresponding vehicle was used to check for any nonspecific effects in all the experiments. The final concentrations of the vehicles, DMSO or saline, pH 13, did not exceed 0.25 and 0.3%, respectively. No effects of the vehicles on the parameters studied were detected.

siRNA Transfection—Twenty four hours after subculturing, rat astrocytes were transfected with specific siRNA sequences TARGETplus™ SMARTpool siRNA from Thermo Fisher Scientific Dharmacon Products (Lafayette, CO). TARGETplus™ SMARTpool siRNA directed against NFκB p65 (L-0800033-01, Rat RelA, NM_199267), NADPH oxidase flavocytochrome b558 gp91(phox) (J-093524), COX-1 (19224, PTGS1), and against the mouse MAPKs MAPK1 (26413, Erk2, NM_011949), MAPK10 (26414, JNK3, NM_009158), and MAPK14 (24416, p38, NM_011951). ON-TARGETplus nontargeting siRNA (D-001810-01) was used as a negative control (nonsilencing). These siRNAs were predesigned by the maker to minimize off-side effects (23), and they were used at 100 nM and transfected with Oligofectamine™ (Invitrogen), as described previously (23). Astrocytes were used 4 days after siRNA transfection. The silencing effect was verified by RT-PCR and/or Western blotting.

Western Blotting—Astrocytes were lysed in buffer containing protease inhibitors. Twenty μg of protein extract were resolved by SDS-PAGE, and proteins were transferred to a polyvinylidene difluoride membrane. Rabbit polyclonal antibodies were used against the following: COX-2 (160126, Cayman Chemical) diluted 1:500; thromboxane synthase (TS) (ab39362, Abcam, Cambridge, UK) diluted 1:1,000; microsomal prostaglandin E synthase-1, PGES-1 (AS03 031, Agrisera, Vännas, Sweden) diluted 1:1,000; c-Jun NH_2-terminal kinase (JNK) (J4500, Sigma), and p38 MAPK (M0800, Sigma) both diluted 1:10,000. A goat polyclonal antibody against COX-1 (Santa Cruz Biotechnology, Santa Cruz, CA) was used diluted 1:1,000. Mouse monoclonal antibodies were used against ERK1/2 (610123, BD Biosciences) diluted 1:50,000 and against β-tubulin (T4026, Sigma) diluted 1:50,000, which was used as control for protein gel loading. Antibodies were diluted in Tris-buffered saline containing 0.5% Tween 20 and were incubated overnight at 4 °C. On the following day, the membranes were incubated with horseradish peroxidase-conjugated goat anti-mouse IgG (Bio-Rad) diluted 1:1,000 or goat anti-rabbit IgG (Amersham Biosciences) 1:2,000 for 2 h at room temperature. The blots were developed with the use of a chemiluminescent substrate (ECL Western blotting Analysis System; Amersham Biosciences).

Immunocytochemistry—Astrocytes were seeded on polylysine-coated coverslips. Cells were washed in PBS and fixed in 4% paraformaldehyde for 30 min. Cells were permeabilized with 0.2% Triton X-100 (Sigma) in PBS for 10 min, blocked with 10% goat or horse serum in PBS for 1 h, and incubated overnight at 4 °C with one of the following primary antibodies: a rabbit polyclonal antibody against Iba-1 (019-19741, Wako Chemicals GmbH, Neuss, Germany) diluted 1:1,000 or a monoclonal antibody against GFAP (G3893, Sigma) diluted 1,1000. The next day, cells were washed and incubated with green fluorescence Alexa Fluor® 488 dye-labeled goat anti-rabbit IgG antibody and Alexa Fluor® 546 goat anti-mouse IgG diluted 1,1000 (Molecular Probes) for 1 h at room temperature. Thereafter, astrocytes were stained with Hoechst to visualize the nuclei. The coverslips were mounted onto microscope slides using Mowiol mounting medium (Calbiochem, Merck). Observations were performed with an Olympus IX70 fluorescence microscope.

For immunohistochemistry in brain tissue, animals were perfused through the heart with saline followed by paraformaldehyde (4%) in phosphate buffer, pH 7.4. The brain was removed, post-fixed with paraformaldehyde overnight, and then kept in phosphate buffer before slicing it in a vibratome to obtain 30-μm-thick coronal sections. Brain sections were cryoprotected in a solution containing glycerol and were kept frozen at −20 °C. Immunohistochemistry was performed free-floating with vibratome sections, as reported previously (25). Endogenous peroxidases were blocked with 3% hydrogen peroxide and 10% methanol in PBS for 25 min. Sections were incubated for 2 h in 3% normal horse or goat serum for mouse monoclonal or rabbit polyclonal antibodies, respectively, to block unspecific

TABLE 1
List of primer sequences for mouse and rat PCR
F means forward, and R means reverse.

	Primer sequence 5′→3′	Accession no.	Amplicon length	Region
			bp	
Mouse				
TNF-α	F, GGGGCCACCACGCTCTTCTGTC	NM_013693	155	Exon 1
	R, TGGGCTACGGGCTTGTCACTCG			Exon 3
Cox-2	F, CCACTTCAAGGGAGTCTGGA	NM_011198.3	187	Exon 3
	R, AGTCATCTGCTACGGGAGGA			Exon 4
Cox-1	F, GTGCTGGGGCAGTGCTGGAG	NM_008969.3	281	Exon 1
	R, TGGGGCCTGAGTAGCCCGTG			Exon 3
mPGES-1	F, AGGCCAGATGAGGCTGCGGA	NM_002415.2	195	Exon 1
	R, AGCGAAGGCGTGGGTTCAGC			Exon 3
PGIS	F, GTGGAGGCCTCACCACGCAC	NM_008968	305	Exon 5
	R, CCCGGGCCTGCATCTCCTCT			Exon 6
TS	F, CACACGGGAGGCAGCACAGG	NM_0011539.3	194	Exon 10
	R, GGGCCAGCTCCAAAGGGCAG			Exon 11
CD11b	F, AAGCAGCTGAATGGGAGGAC	NM_001082960	190	Exon 7
	R, GAATGACCCCTGCTCTGTCT			Exon 8
RPL14	F, GGCTTTAGTGGATGGACCCT	NM_025974	143	Exon 3
	R, ATTGATATCCGCCTTCTCCC			Exon 4
Rat				
Cox-2	F, GATTGACAGCCCACCAACTT	NM_017232	149	Exon 4
	R, CGGGATGAACTCTCTCCTCA			Exon 5
TNF-α	F, GGGGCCACCACGCTCTTCTGTC	NM_012675.3	155	Exon 1
	R, TGGGCTACGGGCTTGTCACTCG			Exon 3
RPL14	F, TCTTTGCCTATGTCAGAGGA	NM_022949	144	Exon 3
	R, GATAGGTATCTTAATTCGAGTCCC			Exon 4

binding sites, washed in T-PBS (PBS containing 0.5% Triton X-100), and incubated overnight at 4 °C with either mouse monoclonal antibody against COX-1 (160110, Cayman Chemical) diluted 1:100, or rabbit polyclonal anti-COX-2 antibody (160126, Cayman Chemical) diluted 1:500. Thereafter, the sections were rinsed in T-PBS and incubated for 1 h with a biotinylated secondary antibody (1:200, Vector Laboratories), followed by incubation with 1% avidin-biotin-peroxidase complex (ABC kit, Vector Laboratories). The reaction was visualized with 0.05% diaminobenzidine in 0.03% hydrogen peroxide in PBS. Double immunohistochemistry was carried out following the first immunoreaction with COX-1 or COX-2. The second primary antibodies used were as follows: a rabbit polyclonal antibody against GFAP (Z0334, DakoCytomation) diluted 1:500, which labels astroglia, or a rabbit polyclonal antibody against Iba-1 (as above) diluted 1:500 to detect microglia. Sections were then incubated with the avidin-biotin complex, washed with 0.01 M sodium phosphate buffer, pH 6, and preincubated for 10 min with 0.01% benzidine dihydrochloride and 0.025% sodium nitroferricyanide in 0.01 M sodium phosphate buffer, pH 6. The reaction was developed with this solution containing 0.005% H_2O_2. Immunoreaction controls included omission of the first or second primary antibodies. The induction of COX-2 in microglia and in astrocytes was assessed by counting the number of $GFAP^+$ and of Iba-1^+ cells expressing COX-2 in the ipsilateral striatum. Microscopic photographs (×20 objective) of three areas surrounding the injection site were taken per brain section in three brain sections per animal. The proportion of microglia (Iba-1^+) and of astroglia ($GFAP^+$) expressing COX-2 was calculated in each photograph, and the average value of all the photographs per animal was calculated. Values are expressed as the mean of four animals treated with LPS and three animals treated with PBS.

Real Time RT-PCR—Total RNA was extracted using the PureLink RNA kit (Invitrogen). RNA quantity and purity were determined using ND-1000 microspectrophotometer (NanoDrop Technologies, Wilmington, DE). One μg of total RNA was reverse-transcribed using a mixture of random primers (High Capacity cDNA reverse transcription kit, Applied Biosystems). Real time quantitative RT-PCR analysis was carried out by SYBR Green I dye detection (11761500, Invitrogen) using the iCycler iQTM Multicolor real time detection system (Bio-Rad). PCR primers were designed with the aid of Primer3 software to bridge the exon-intron boundaries within the gene of interest to exclude amplification of contaminating genomic DNA. Several genes were assayed as loading controls (*Hprt1, Sdha, Ywhaz,* and *Rpl14*). *Rpl14* was the control gene showing the best stability after LPS treatment and was chosen for normalization. Primers (see list in Table 1) were purchased from IDT (Conda, Spain). Optimized thermal cycling conditions were as follows: 1 min at 50 °C, 8 min, and 30 s at 95 °C and 40 cycles of 15 s at 95 °C and 30 s at 60 °C in which an optical acquirement were performed. Data were collected after each cycle and were graphically displayed (iCycler iQTM real time detection system software, version 3.1, Bio-Rad). Melt curves were performed upon completion of the cycles to ensure absence of nonspecific products. Quantification was performed by normalizing cycle threshold (*Ct*) values with the Rpl14 control gene *Ct*, and analysis was carried out with the $2-\Delta\Delta CT$ method (26).

ELISAs—The cellular supernatant was used in ELISAs to measure the concentration of: prostaglandin E_2 (PGE_2, 900-001), thromboxane B_2 (TxB_2, 900-002), and 6-keto-prostaglandin F1α (PG F1α, 900-004) (Assay Designs, Ann Arbor, MI).

Statistical Analyses—One-way analysis of variance was used for comparisons between multiple groups, after testing for normality, followed by the post hoc Bonferroni test. Comparison between two groups was carried out with the *t* test after verifying normal distribution; otherwise, the nonparametric Mann Whitney test was used. Linear or nonlinear regression analyses

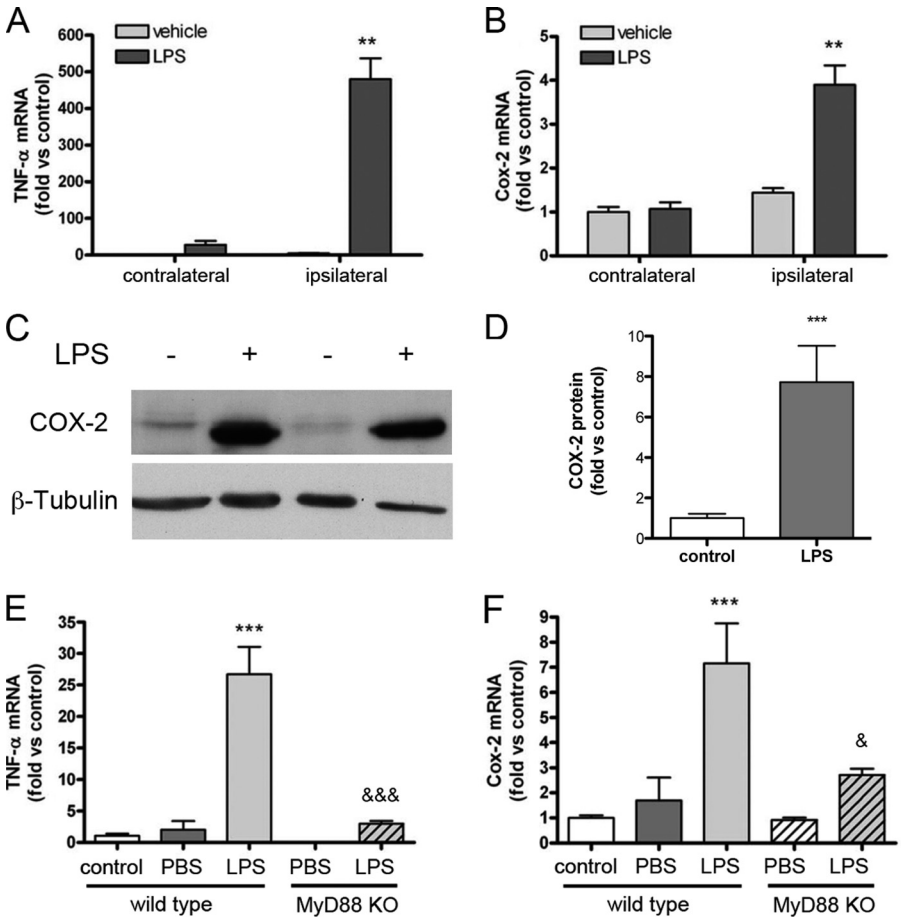

FIGURE 1. **LPS administration to the rat brain induced COX-2 in glial cells.** Rats received an intrastriatal injection of LPS (5 μl, 1 μg/μl) or the vehicle (PBS), and the brain tissue was obtained 8 h later to study mRNA and protein expression. *A* and *B,* rats injected with LPS show a very pronounced increase in the expression of *Tnf-α* and *Cox-2* mRNA in the ipsilateral hemisphere compared with that in animals receiving the vehicle or in the contralateral hemisphere (n = 3–5 rats per group). *C,* COX-2 protein was detected by Western blotting in the ipsilateral hemisphere 8 h after LPS. *D,* semi-quantification of COX-2 band intensity indicated a significant increase of COX-2 expression after LPS (n = 3 rats per group). *E* and *F,* expression of *Tnf-α* and *Cox-2* mRNA in the ipsilateral hemisphere of mice 8 h after striatal injection of LPS (0.7 μl, 1 μg/μl) is powerfully attenuated in MyD88-deficient mice (MyD88 KO) compared with the WT (n = 3–4 per group). Control animals received intrastriatal injection of the vehicle (PBS). *One symbol*, $p < 0.05$; *two symbols*, $p < 0.01$; *three symbols*, $p < 0.001$. Symbols indicate comparison *versus* either (*) control or (&) LPS WT.

were used for curve fits as appropriate using GraphPad software.

RESULTS

Intracerebral Administration of LPS Induces Cox-2 in Microglia and Astroglia—Intracerebral administration of LPS to rats induced mRNA expression of *Tnf-α* (Fig. 1*A*) in the ipsilateral hemisphere at 8 h. LPS also increased the expression of *Cox-2* mRNA (Fig. 1*B*) and COX-2 protein (Fig. 1, *C* and *D*). LPS induces TLR-4 activation and recruitment of the MyD88 adaptor protein that mediates activation of the transcription factor NFκB and induction of target genes, such as the pro-inflammatory cytokine TNF-α (21). In agreement with this, MyD88 KO mice did not show induction of *Tnf-α* (Fig. 1*E*) or *Cox-2* (Fig. 1*F*) mRNA in the ipsilateral hemisphere after LPS, indicating that induction of both genes was MyD88-dependent.

LPS up-regulated the expression of *Iba-1* mRNA in the ipsilateral hemisphere at 8 h suggesting microglial activation, whereas expression of *Gfap* mRNA was not modified at this time point (supplemental Fig. 3). However, by immunohistochemistry (Fig. 2), we detected a strong induction of COX-2, not only in microglia (Fig. 2, *A–D*) but also in astrocytes (Fig. 2, *E–G*) of the ipsilateral hemisphere 8 h after LPS. Quantification of the immunohistochemistry showed increased numbers of COX-2 immunoreactive microglia (Iba-1) and astrocytes (GFAP) after LPS (Fig. 2, *P* and *Q*). COX-1 was expressed under basal conditions preferentially in microglia (Fig. 2, *H–K*) and, with a lower intensity, in astroglia (Fig. 3, *L–O*), and it was not up-regulated by LPS (Fig. 2, *H–O*).

We then undertook an *in vitro* study in purified cultures of astroglia treated with LPS to unravel the mechanisms underlying COX-2 induction and prostanoid release induced by TLR-4 activation, and the effects of deficiency or inhibition of either COX-1 or COX-2.

Regulation of COX-2 Expression in Astrocytes Challenged with LPS—LPS induced *Tnf-α* (Fig. 3*A*) and *Cox-2* (Fig. 3*B*) mRNA and protein expression (Fig. 3, *C* and *D*) in cultured astrocytes, as it did *in vivo* (Fig. 1, *A–D*). The transcription factor NFκB was involved in COX-2 induction because silencing the p65 subunit of NFκB with siRNA attenuated *Cox-2* mRNA induction (Fig. 3*E*). However, this effect was not observed by silencing other genes, such as the gp91 subunit of

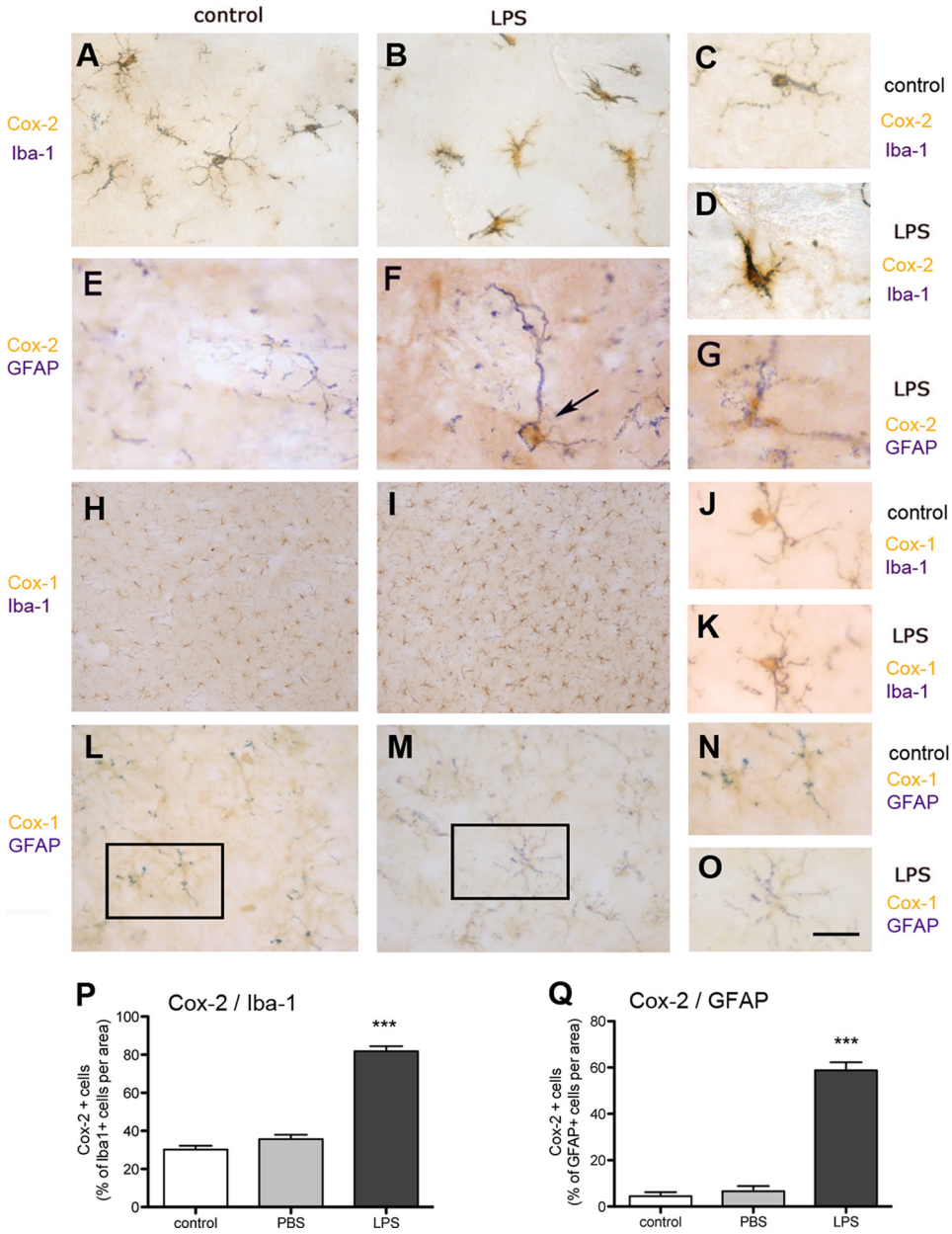

FIGURE 2. **COX-2 is induced in astrocytes and microglia after LPS in the rat brain.** Immunohistochemistry against COX-2 (*brown* in *A–G*) and COX-1 (*brown* in *H–O*) in control rat brain (*A, C, E, H, J, L,* and *N*) and after LPS (*B, D, F, G, I, K, M,* and *O*) shows co-localization of COX-2 with markers of microglia (*Iba-1*) (*B* and *D*) and astroglia (*GFAP*) (*arrow* in *F* and *G*) (*dark blue/purple*), whereas COX-1 is predominantly expressed in microglia (*H–J*) and to a lower extent in astroglia (*L–N*), and it is not up-regulated after LPS (*I, K, M,* and *O*). The areas indicated with *rectangles* in *L* and *M* are magnified in *N* and *O*, respectively. *Bar scale,* 30 μm (*A–G, J–K, N,* and *O*); 60 μm (*L* and *M*); 120 μm (*H* and *I*). *P* and *Q,* quantification of the proportion of microglia and astroglia cells expressing COX-2. Values are expressed as % of total Iba-1+ microglia (*P*) or GFAP+ astroglia (*Q*). $n = 4$–5 LPS-treated mice and $n = 3$ mice injected with PBS. Controls are taken as the contralateral nonaffected hemispheres, $n = 7$. One-way analysis of variance, and *** indicates $p < 0.001$.

NADPH oxidase complex (Fig. 3*E*) that was reported to mediate COX-2 induction after LPS in microglia (27). The involvement of NFκB in mediating the induction of COX-2 after LPS was further substantiated by the use of the inhibitor PDTC, which attenuated the effect of LPS (Fig. 3*F*). We then used astrocytes from mice deficient in MyD88 or corresponding WT mice to explore whether COX-2 induction was dependent on the MyD88 pathway in these cells, as observed previously *in vivo* (Fig. 1, *E* and *F*). LPS failed to induce *Tnf-α* mRNA in MyD88-deficient astrocytes (Fig. 3*G*), which did not express *Cox-2* mRNA (Fig. 3*H*) or protein (Fig. 3*I*). Therefore, COX-2 induction after LPS is dependent on MyD88 and NFκB.

MAPKs participate in LPS signaling (28) and can mediate COX-2 induction (29). We used specific inhibitors of MAPK pathways to unravel their contribution in COX-2 up-regulation after LPS in astrocytes. *Cox-2* mRNA induction was severely reduced by the p38 inhibitor SB23906 and by the JNK inhibitor SP600125 but not by the MEK inhibitor U0126 (Fig. 4*A*). Likewise, COX-2 protein expression 8 h after LPS was very sensitive to SB239063 (from 1 μM) (Fig. 4*B*) and SP600125 (from 10 μM) (Fig. 4*C*), whereas U0126 (1–25 μM) had a negligible effect (Fig. 4*D*). This finding was validated with another MEK inhibitor, PD98059 (from 10 to 40 μM) (Fig. 4*D*). The same result was found at 4 h (Fig. 4*E*). In agreement with this, the production of

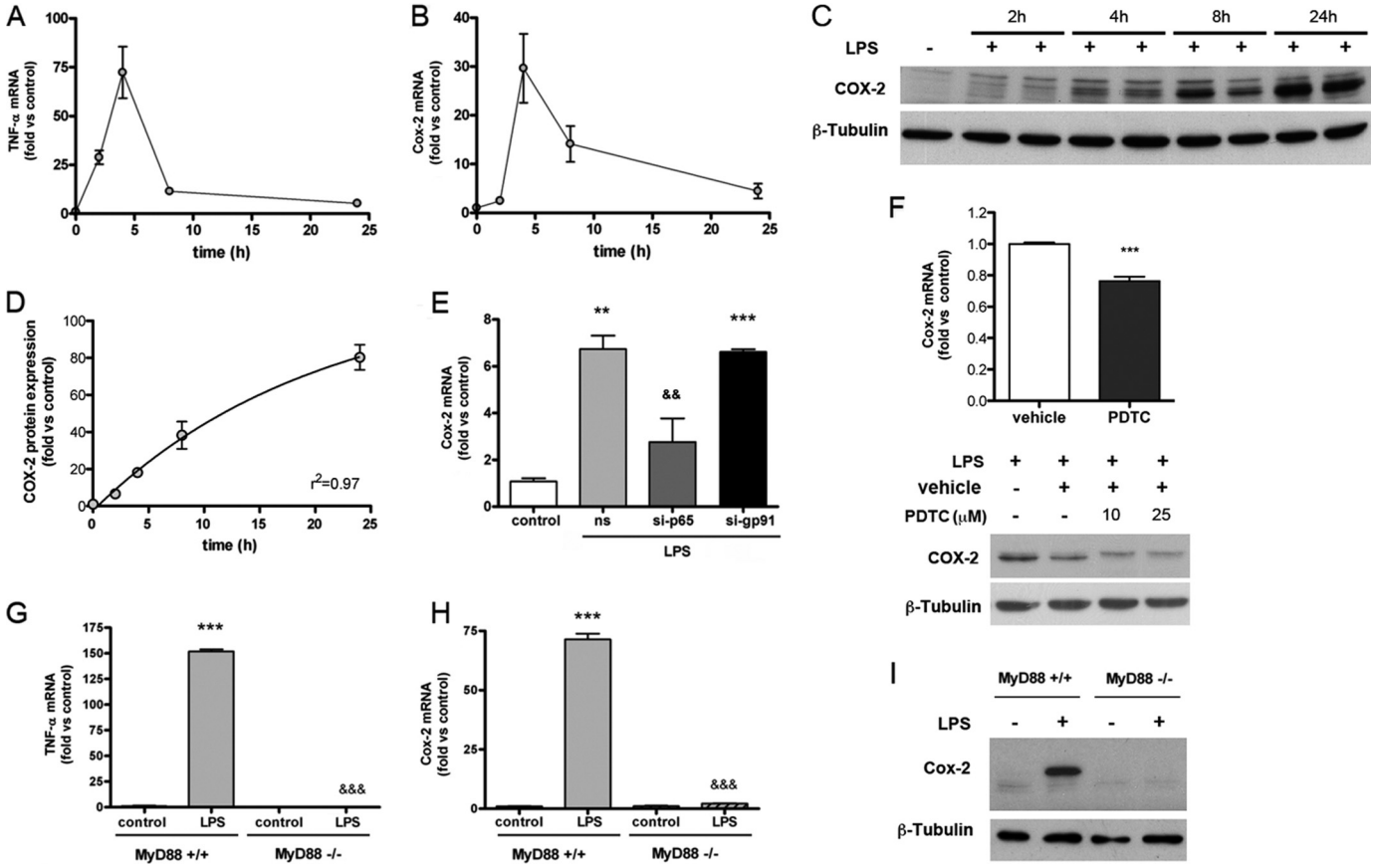

FIGURE 3. **COX-2 induction after LPS is dependent on NFκB and MyD88 pathways.** LPS (10 ng/ml) was added to rat (*A, B,* and *E*) or mouse (*C–D* and *F–I*) astrocyte cultures, and mRNA/proteins were studied at different time points (*A–D*) or at 4 h. *A* and *B,* time course expression of *Tnf-α* and *Cox-2* mRNA after LPS. *C,* time course of COX-2 protein expression after LPS was assessed by Western blotting. *D,* semi-quantification of COX-2 band intensity in *C*. Data were fit to the curve with nonlinear regression analysis (one-phase exponential association). The goodness of the fit was assessed by r^2. *E,* cells were transfected with Oligofectamine carrying small interference RNA (siRNA) against either the p65 subunit of NFκB (si-p65) or the gp91 subunit of NADPH (si-gp91). A nonsilencing (*ns*) scramble double-stranded RNA was used as control. In these cells, the induction of *Cox-2* mRNA is dependent on NFκB. *F,* NFκB inhibitor PDTC also prevents *Cox-2* mRNA and protein induction after LPS. *G–I,* induction of *Tnf-α* (*G*) and COX-2 (*H*) mRNA is strongly reduced in astrocytes deficient in MyD88 (MyD88$^{-/-}$) *versus* the wild type (MyD88$^{+/+}$). Likewise, COX-2 protein is detected by Western blotting in WT cells but not in MyD88-deficient cells (*I*). β-Tubulin is shown in the Western blots as a loading control. Values are expressed as the mean ± S.E. of $n = 3$ per condition. *One symbol*, $p < 0.05$; *two symbols*, $p < 0.01$; *three symbols*, $p < 0.001$. Symbols indicate comparison *versus* either (*) control or (&) LPS (WT or treatment control).

PGE_2, as assessed by ELISA 8 h after LPS, was reduced by p38 and JNK inhibitors but not after MEK inhibition (Fig. 4*F*).

We then silenced the expression of MAPK1 (ERK2), MAPK10 (JNK3), and MAPK14 (p38) using siRNA. Western blotting (Fig. 4*G*) showed that siRNAs reduced the corresponding protein expression by 65–70%. Silencing p38 and JNK3 attenuated the expression of Cox-2 mRNA and protein, but no significant effects were observed after silencing MAPK1 (Fig. 4, *H–J*). Therefore, we can conclude that induction of COX-2 expression after LPS is strongly dependent on the MyD88 pathway NFκB and on p38 and JNK pathways.

Regulation of COX-1 Expression after LPS—We also examined whether the expression of constitutive COX-1 was affected by LPS. The expression of *Cox-1* mRNA was significantly reduced 8 h after LPS in WT astrocytes, and the same effect was observed in *Cox-2* KO cells (Fig. 5*A*), which we verified did not express *Cox-2* mRNA (Fig. 5*B*) or protein (Fig. 5, *C* and *D*). Although the reduction of *Cox-1* mRNA by LPS was already seen at 4 h (Fig. 5, *G* and *I*), COX-1 protein expression was unaltered at this time point, but a slight reduction was seen at 8 and 24 h (Fig. 5, *E* and *F*). The delay in the reduction of the amount of COX-1 protein after the decreased expression of *Cox-1* mRNA might be due to the presence of the constitutive protein that needs to follow its turnover before reductions in mRNA can be translated into protein decreases.

LPS-induced reduction of COX-1 was not prevented by MAPK inhibition (Fig. 5, *G* and *H*) or by silencing MAPK expression with siRNA (Fig. 5, *I* and *J*). However, LPS-induced down-regulation of Cox-1 mRNA was dependent on the MyD88 pathway because LPS did not reduce it in MyD88 KO mice (Fig. 5*K*). To better substantiate this finding, we examined whether down-regulation of COX-1 also occurred *in vivo* in the mouse brain after intracerebral LPS administration. Expression of *Cox-1* mRNA was significantly reduced 8 h after injection of LPS but not after injection of PBS (Fig. 5*L*). This effect was strongly attenuated in MyD88-deficient mice (Fig. 5*L*), supporting that it was MyD88-dependent. PDTC attenuated the reduction of *Cox-1* mRNA induced by LPS in cultured cells, suggesting that NFκB was involved (Fig. 5*M*).

Because COX-1 and COX-2 expression responded in an opposite way to the LPS challenge, we examined whether Cox-

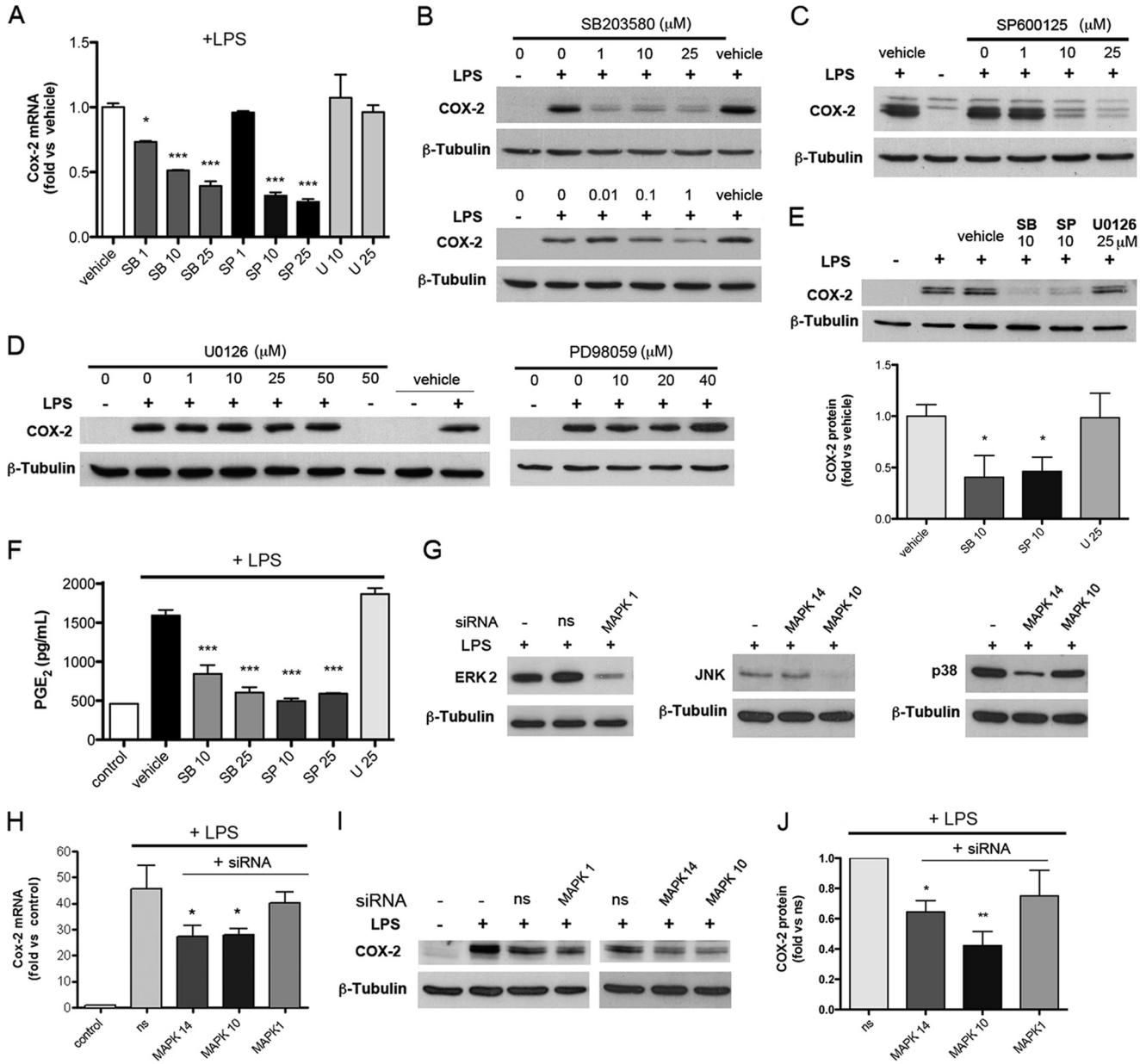

FIGURE 4. **LPS-induced COX-2 is dependent on p38 and JNK MAPK.** LPS (10 ng/ml) was added to mouse astrocyte cultures, and mRNA/proteins were studied at 4 or 8 h. *A,* astrocytes were treated with LPS in the presence or absence (−) of the indicated doses of MAPK inhibitors (or the vehicle): SB239063 (*SB*), SP600125 (*SP*), and U0126 (*U*), which inhibit the p38, JNK, and MEK pathways, respectively, and *Cox-2* mRNA was studied 4 h after LPS. The results show the involvement of p38 and JNK in LPS-induced *Cox-2* mRNA. *B–D,* COX-2 protein expression 8 h after LPS was inhibited by SB239063 (from 1 to 25 μM) (*B*), and SP600125 (from 10 to 25 μM) (*C*), but not by MEK inhibitors (up to 25 μM U0126 and up to 40 μM PD98059) (*D*). *E,* COX-2 protein 4 h after LPS was also inhibited by p38 and JNK inhibitors but not after MEK inhibition (U0126). *F,* accordingly, SB239063 and SP600125, but not U0126, inhibit the production of PGE_2, as assessed by ELISA in the culture medium 8 h after LPS. *G,* silencing MAPK with siRNA effectively reduces the expression of the corresponding target proteins by 65–70%. *H–J,* silencing MAPK10 (JNK3) or MAPK14 (p38), but not MAPK1 (ERK2), reduces *Cox-2* mRNA (*H*) and protein (*I* and *J*) *versus* treatment with nonsilencing (*ns*) RNA 4 h after LPS. β-Tubulin is shown in the Western blots as a loading control. Values are expressed as the mean ± S.E. of $n = 3$ per condition in at least three independent experiments. *One symbol*, $p < 0.05$; *two symbols*, $p < 0.01$; *three symbols*, $p < 0.001$.

1-deficient mice (Fig. 5*N*) showed up-regulation of *Cox-2* mRNA (Fig. 5*O*) and protein (Fig. 4*O*) after LPS, which they did. These results support that although LPS strongly induces COX-2, it represses the expression of COX-1, and both responses are dependent on the MyD88 pathway, whereas p38 and JNK MAPK are involved in up-regulating COX-2 but not in down-regulating COX-1.

LPS Modifies the Expression of Prostaglandin Isomerases—The types of prostanoids that are produced after COX activation depend on the action of specific prostanoid isomerases, *i.e.* the enzymes responsible for the production of prostanoids from COX-derived PGH_2. LPS induced strong mRNA expression of one of the isoforms of PGE_2 synthase, the microsomal PGE synthase-1 (*mPges-1*) (Fig. 6*A*), in WT and *Cox-1-* or *Cox-2*-deficient cells. Like for COX-2, induction of mPGES-1 after LPS was dependent on the MyD88 pathway because MyD88-deficient cells showed no increase of *mPges-1* mRNA expression (Fig. 6*B*). These findings show that LPS up-regulates the expression of *mPges-1* through the MyD88 pathway, in a manner coordinated with the induc-

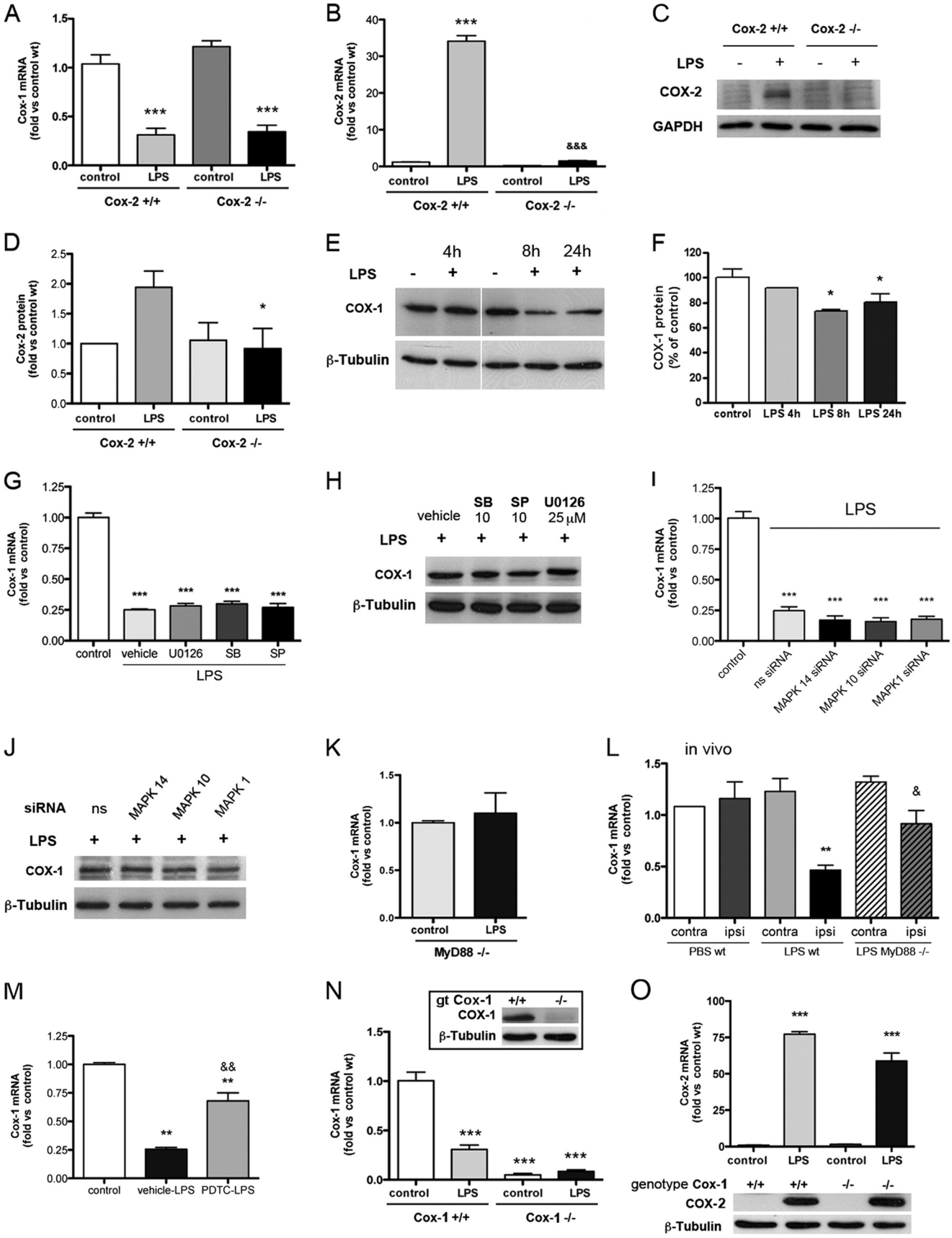
A
Cox-1 mRNA (fold vs control wt)
control
LPS
Cox-2 +/+
Cox-2 -/-
B
Cox-2 mRNA (fold vs control wt)
C
Cox-2 +/+
Cox-2 -/-
LPS
COX-2
GAPDH
D
Cox-2 protein (fold vs control wt)
E
4h
8h
24h
COX-1
β-Tubulin
F
COX-1 protein (% of control)
LPS 4h
LPS 8h
LPS 24h
G
Cox-1 mRNA (fold vs control)
vehicle
U0126
SB
SP
H
SB
SP
U0126
25 μM
I
ns siRNA
MAPK 14 siRNA
MAPK 10 siRNA
MAPK1 siRNA
J
siRNA
ns
MAPK 14
MAPK 10
MAPK 1
K
MyD88 -/-
L
in vivo
contra
ipsi
PBS wt
LPS wt
LPS MyD88 -/-
M
vehicle-LPS
PDTC-LPS
N
gt Cox-1
+/+
-/-
Cox-1 +/+
Cox-1 -/-
O
genotype Cox-1

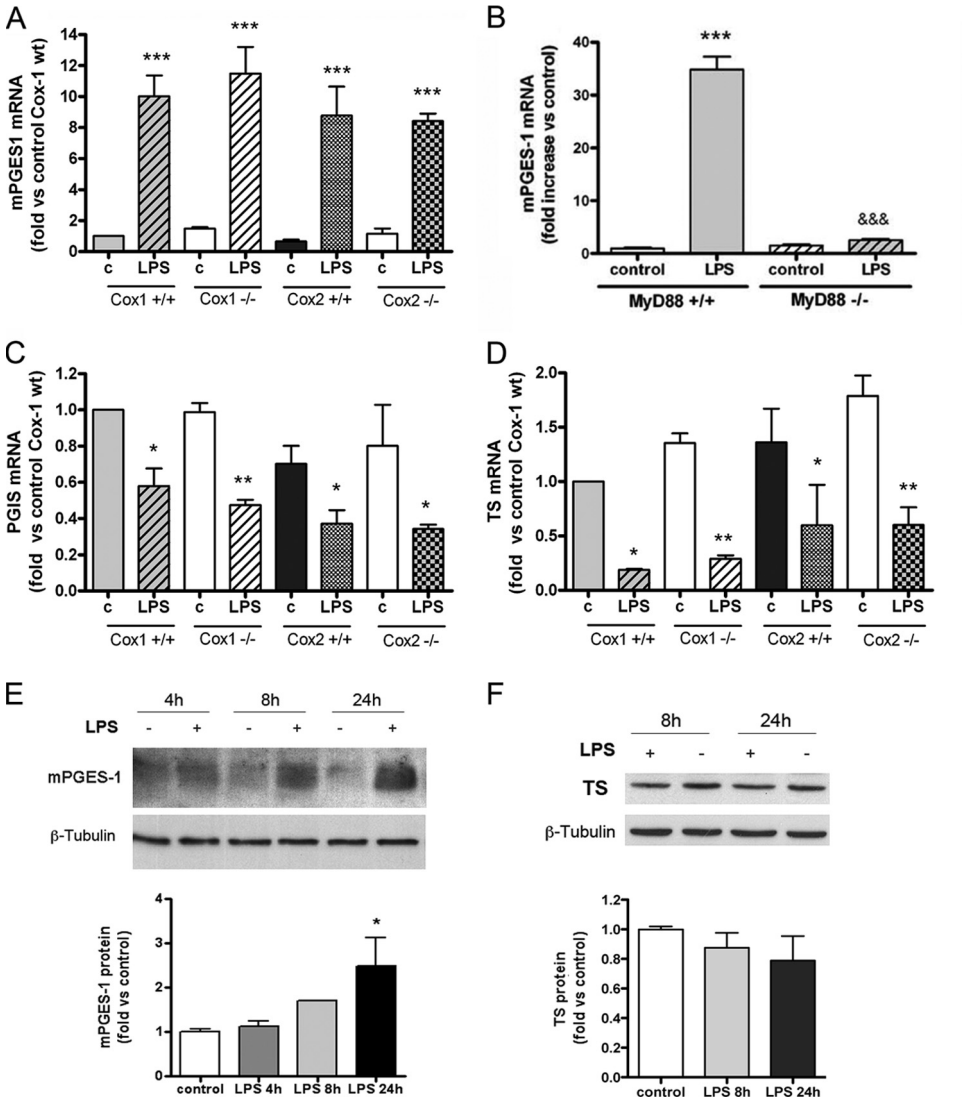

FIGURE 6. **LPS induces expression of *mPges-1* mRNA but not of the enzymes that synthesize other prostanoids.** Astrocytes of *Cox-1* or *Cox-2* KO mice (−/−) and their respective wild type (+/+) astrocytes were treated with LPS (10 ng/ml), and mRNA was extracted at 8 h. *A,* LPS strongly induces microsomal PGE_2 synthase-1 (mPGES1) mRNA in the different genotypes. *c*, control. *B,* induction of *mPges1* mRNA after LPS is dependent on the MyD88 pathway, as shown by lack of *mPges-1* mRNA up-regulation in MyD88-deficient ($MyD88^{-/-}$) cells after LPS. *C* and *D,* expression of prostacyclin synthase (*PGIS*) mRNA (*C*) and that of TS mRNA (*D*) is reduced after LPS in all genotypes. *E* and *F,* accordingly, in astrocytes from C57 WT mice, LPS significantly up-regulates the expression of mPGES1 protein (*E*), although TS protein shows a nonsignificant tendency to progressively decrease with time *versus* controls (*F*). $n = 3$ for each genotype. *One symbol*, $p < 0.05$; *two symbols*, $p < 0.01$; *three symbols*, $p < 0.001$. * indicates comparison *versus* control; & indicates comparison *versus* LPS in WT.

tion of COX-2, to strongly generate PGE_2. In contrast to the above findings, LPS down-regulated the expression of prostacyclin synthase (*Pgis*) mRNA (Fig. 6*C*) and, to a greater extent, thromboxane synthase (*Ts*) mRNA (Fig. 6*D*). Accordingly, although after LPS the expression of mPGES-1 protein significantly increased (Fig. 6*E*), the expression of TS protein tended to be progressively lower than in controls (Fig. 6*F*). The latter effects on TS paralleled the down-regulation of COX-1 expression after LPS (Fig. 5, *A* and *E*), suggesting common regulatory pathways.

LPS Exposure Induces Prostanoid Production in Astrocytes—COX enzymes metabolize arachidonic acid to prostaglandins PGG_2 and PGH_2 that are rapidly converted by cell-specific prostaglandin isomerases into different prostanoids, including

FIGURE 5. **LPS down-regulates COX-1 expression in astrocytes.** Cultured mouse astrocytes were treated with LPS (10 ng/ml) for 4, 8, or 24 h. *A, Cox-1* mRNA expression is down-regulated 8 h after LPS in WT (+/+) and *Cox-2*-deficient cells (−/−). *B–D,* lack of expression of *Cox-2* mRNA and protein in *Cox-2* KO cells is shown compared with WT. *E* and *F,* COX-1 protein expression decreases from 8 h after LPS but not at 4 h. *G–J,* down-regulation of COX-1 after LPS is not MAPK-dependent because it is not altered by MAPK inhibitors (*G* and *H*) or by silencing the indicated MAPK (*I* and *J*) (*ns* indicates treatment with control nonsilencing RNA). *K,* LPS-induced down-regulation of *Cox-1* is not observed in MyD88-deficient cells, suggesting that it is MyD88-dependent. *L,* intracerebral administration of LPS to mice also induces a reduction of *Cox-1* mRNA expression in the ipsilateral (*ipsi*) hemisphere 8 h after LPS, and this effect is strongly attenuated in MyD88-deficient mice. *contra*, contralateral. *M,* NFκB inhibition with PDTC (10 μM) significantly attenuates the reduction of *Cox-1* mRNA induced by LPS at 4 h in cultured astrocytes. *N,* compared with WT cells, low levels of *Cox-1* mRNA are found in *Cox-1*-deficient cells, and COX-1 protein is not detected in these cells by Western blotting (*inset*). *O, Cox-1* KO cells produce *Cox-2* mRNA and protein 4 and 8 h after LPS, respectively. β-Tubulin is shown as a loading control. $n = 3$ per condition in each result. *One symbol*, $p < 0.05$; *two symbols*, $p < 0.01$; *three symbols*, $p < 0.001$. *Symbols* indicate comparison *versus* either (*) control or (&) LPS (WT or untreated).

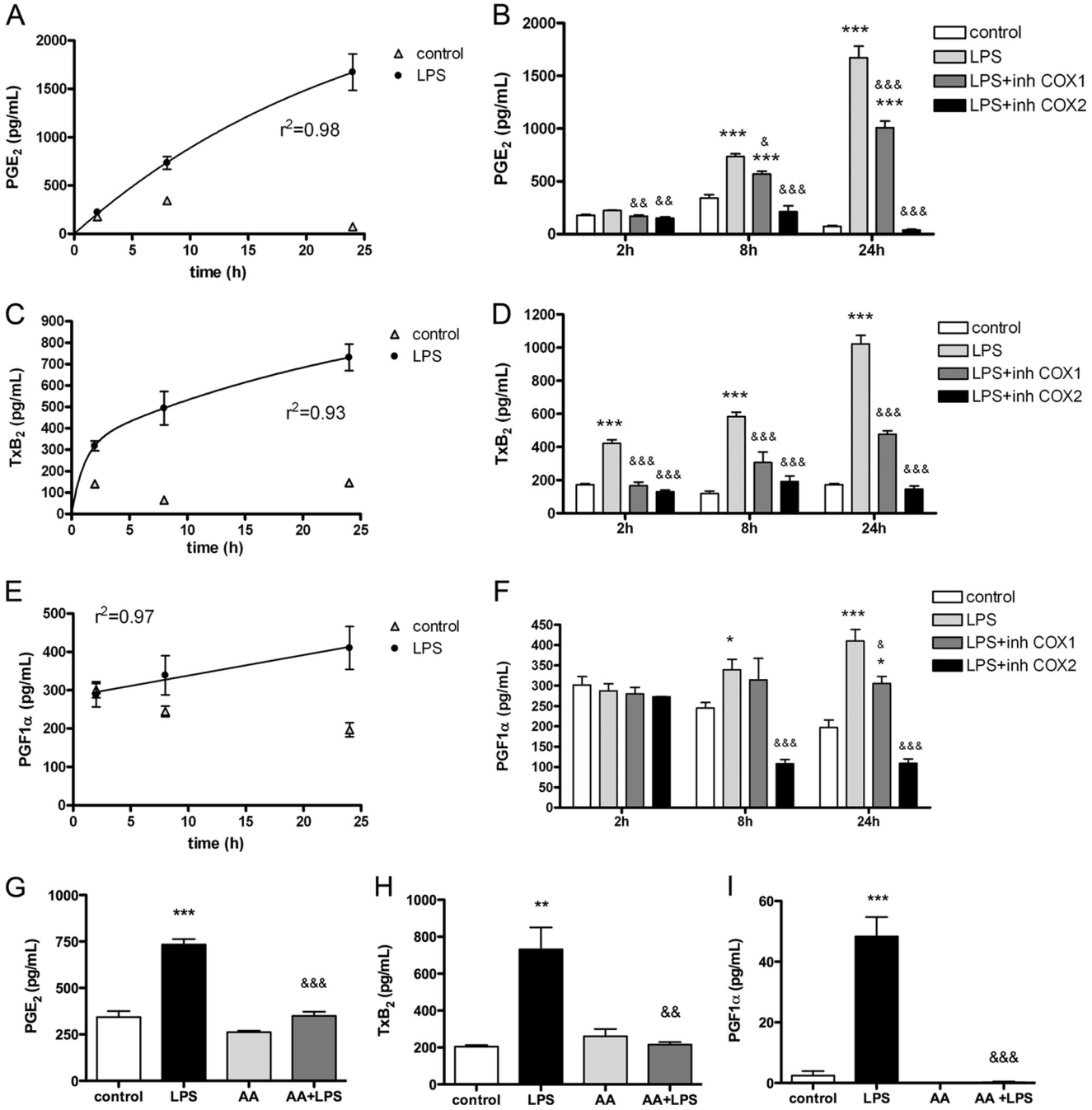

FIGURE 7. **LPS induces secretion of prostanoids to the culture medium.** Purified cultures of rat astrocytes were exposed to LPS (10 ng/ml) for different times, and the medium was collected and studied by ELISA. ELISAs were carried out in five independent experiments, and *curves* from representative experiments are shown. *A*, time course of PGE_2 concentrations in the culture medium. *B*, LPS does not induce PGE_2 in the presence of the Cox-2 inhibitor NS-398 (3 μM), and PGE_2 concentration is lower in the presence of the Cox-1 inhibitor SC-560 (10 nM). *C*, time course of TxB_2 as an indicator of the generation of TxA_2. *D*, NS-398 strongly reduces the production of TxB_2 induced by LPS, whereas SC-560 attenuates the effect of LPS. *E*, time course of PGF-1α concentration to indirectly assess the formation of prostacyclin. *F*, NS-398 strongly reduces the concentration of PGF1-α in the medium, whereas some reduction is observed with the Cox-1 inhibitor (*inh*) SC-560. *G–I*, $cPLA_2$ inhibitor arachidonyltrifluoromethyl ketone (2 μM) completely abrogates LPS-induced prostanoid formation as assessed at 8 h after LPS exposure. *AA*, arachidonic acid. *One symbol*, $p < 0.05$; *two symbols*, $p < 0.01$; *three symbols*, $p < 0.001$. * indicates comparison *versus* control. & indicates comparison *versus* LPS alone. Data (mean ± S.D.) were fit to the curve with nonlinear regression analysis (one-phase exponential association) in *A* and *C*, and with linear regression in *E*. The goodness of the fit was assessed by r^2.

PGE_2, $PGF_{2\alpha}$, prostacyclin (PGI_2), and thromboxane A_2 (TxA_2), among others. We examined the profile of several prostanoids induced by LPS in the culture medium of rat astrocytes by ELISAs. TxA_2 has a half-life of only a few seconds (30), and its production is typically assessed by measuring TxB_2, which is a stable metabolite. PGI_2 has a half-life of 60 min in plasma, but it is stable for only a few minutes in buffer (30), and its production is typically monitored by measurement of 6-keto-prostaglandin $F_{1\alpha}$ (PGF1α). LPS caused a very strong accumulation of PGE_2 in the cell culture medium of rat astrocytes from 2 to 24 h (Fig. 7, *A* and *B*), and to a lesser extent it increased the concentration of TxB_2 (Fig. 7, *C* and *D*) and of PGF1α (Fig. 7, *E* and *F*)

at 8 and 24 h. The $cPLA_2$ inhibitor arachidonyltrifluoromethyl ketone fully prevented the production of prostanoids (Fig. 7, *G–I*), suggesting the involvement of $cPLA_2$ in arachidonic acid mobilization after LPS.

Prostanoid Production after LPS Treatment Is Prevented by COX-2 Inhibitors—COX-2 inhibitor NS-398 strongly blocked LPS-induced PGE_2, TxA_2, and PGI_2 production, whereas COX-1 inhibition with SC-560 only partly attenuated the generation of prostanoids after LPS in rat astrocytes (Fig. 7, *B*, *D*, and *F*). These results suggested that COX-2 was the main mediator of prostanoid production after LPS and pointed to a small contribution of COX-1 due to a weak inhibitory effect of SC-560. Although SC-560 is widely used to inhibit COX-1 and specific inhibition of this enzyme has been shown in cell-free systems, cell studies suggest that this compound may also exert some nonspecific inhibitory effects on COX-2 (31). This possible inhibition of COX-2 might explain why we found some partial inhibitory effects of SC-560 on prostanoid production in our system. To further investigate if SC-560 has COX-1-independent effects, we used astrocytes from COX-1-deficient mice. SC-560 significantly ($p < 0.001$) reduced the production of PGE_2, $PGF1\alpha$, and TxB_2 (supplemental Fig. 4) induced by LPS in Cox-1 KO cells, thus indicating that this compound may have COX-1-independent effects.

Prostanoid Production after LPS Treatment Is Dependent on COX-2—We showed above that the induction of COX-2 by LPS was strongly inhibited in MyD88-deficient cells (Fig. 3, *H* and *I*). For this reason, we then examined whether LPS-induced prostanoid production was abrogated in these cells. Compared with the previous findings of prostanoid release after LPS in rat astrocytes, we noticed that mouse astrocytes produced less thromboxane and more prostaglandin than rat astrocytes, although in both species PGE_2 was the prostanoid more abundantly generated in response to LPS. Lack of MyD88 prevented the production of prostanoids after LPS (Fig. 8, *A–C*), thus further supporting that COX-2 was the main mediator of prostanoid production after this challenge. Because COX-2 was not induced in MyD88 KO cells, the slightly higher production of TxB_2 after LPS than in control MyD88 KO cells might be attributable to COX-1 activity and related to the finding that the basal COX-1 expression was not down-regulated after LPS in MyD88 KO cells (Fig. 4*I*).

We then used astrocytes obtained from mice deficient in *Cox-1* or *Cox-2* and their corresponding WT controls to validate the above findings, excluding possible interferences because of nonspecific effects of the drug inhibitors. Astrocytes lacking *Cox-2* did not produce PGE_2 (Fig. 8*D*), PGI_2 (Fig. 8*E*), or TxA_2 (Fig. 8*F*) in response to LPS, thus confirming that COX-2 was the main enzyme involved in the production of prostanoids induced by LPS in astrocytes. Under basal nonstimulated conditions, the concentration of TxB_2 was not reduced in cells lacking *Cox-2* compared with the WT, although they showed very low levels of PGE_2 and $PGF1\alpha$, suggesting that COX-1 is involved in the low basal production of TxA_2 in astrocytes. This is in agreement with the previous observation in MyD88-deficient cells, where LPS did not induce COX-2 but did not down-regulate COX-1 either. These cells showed an increase in the production of TxB_2 after LPS (Fig. 8*C*) that is attributed to the basal activity of COX-1 metabolizing the arachidonic acid newly generated after LPS-induced $cPLA_2$ activation.

Cox-1-deficient cells produced PGE_2 after LPS to a greater extent than the corresponding WT astrocytes (Fig. 8*G*), showing that COX-2 is the enzyme responsible for PGE_2 production and suggesting some negative regulatory effect of COX-1 on PGE_2 production after LPS. Also, LPS increased the production of PGI_2, as assessed by measuring $PGF1\alpha$ (Fig. 8*H*), and TxA_2, as assessed by measuring TxB_2 (Fig. 8*I*), in *Cox-1*-deficient cells suggesting the involvement of COX-2. To add further support to these findings, we silenced *Cox-1* with siRNA (Fig. 8*J*). Under these conditions, a small but significant increase in the production of PGE_2 after LPS was observed (Fig. 8*K*), whereas the production of PGI_2 (Fig. 8*L*) and TxA_2 (Fig. 8*M*) was not altered. Altogether, these results show that COX-1 activity maintains basal production of prostanoids in cultured astrocytes but does not have a major role in the increased production of prostanoids after LPS.

DISCUSSION

These results show that the production of prostanoids induced by LPS in glial cells is essentially mediated by COX-2. The MyD88-dependent pathway and the transcription factor NFκB were involved in *Cox-2* gene expression. In addition, p38 and JNK MAPK pathways influenced *Cox-2* expression, thus revealing a complex regulation of the expression of this gene in response to TLR-4 activation in astroglia. COX-2 induction was accompanied by strong production of PGE_2 and, to a lesser extent, other prostanoids. Several lines of evidence suggest that the COX isoforms are coupled to the activity of the various prostaglandin isomerases favoring the production of certain prostanoids in a cell type-dependent manner (32). The strong production of PGE_2 in astrocytes after LPS is in concordance with the enhanced expression of the microsomal isoform of prostaglandin E synthase-1 (mPGES-1), in agreement with previous findings (33). In addition, here we report that the expression of the *mPges-1* gene after LPS was up-regulated through the MyD88 pathway, like *Cox-2*. Therefore, LPS induces the coordinated expression of COX-2 and mPGES-1, which appeared to be functionally coupled and accounts for the high production and release of PGE_2 in astrocytes, in a manner similar to the responses described in macrophages (34).

In a previous study, induction of COX-2 and mPGES-1 was mainly found in microglia in the substantia nigra 48 h after intracerebral injection of LPS (35). In contrast, we also observed the induction of COX-2 in astrocytes 8 h after LPS injection into the striatum. Besides any regional differences in the reaction to LPS, it is likely that the time course of the glial reaction to this challenge accounts for the observed differences. Increased expression of mPGES-1 has been reported under pathological conditions, *e.g.* in the brain of Alzheimer disease patients (36), and the enzyme is up-regulated in astrocytes stimulated with β-amyloid (37). Also, after intracerebral hemorrhage, strong induction of COX-2 and mPGES-1 was found in astrocytes (38). Therefore, the findings reported here in cultured cells might be relevant to certain neuropathological conditions.

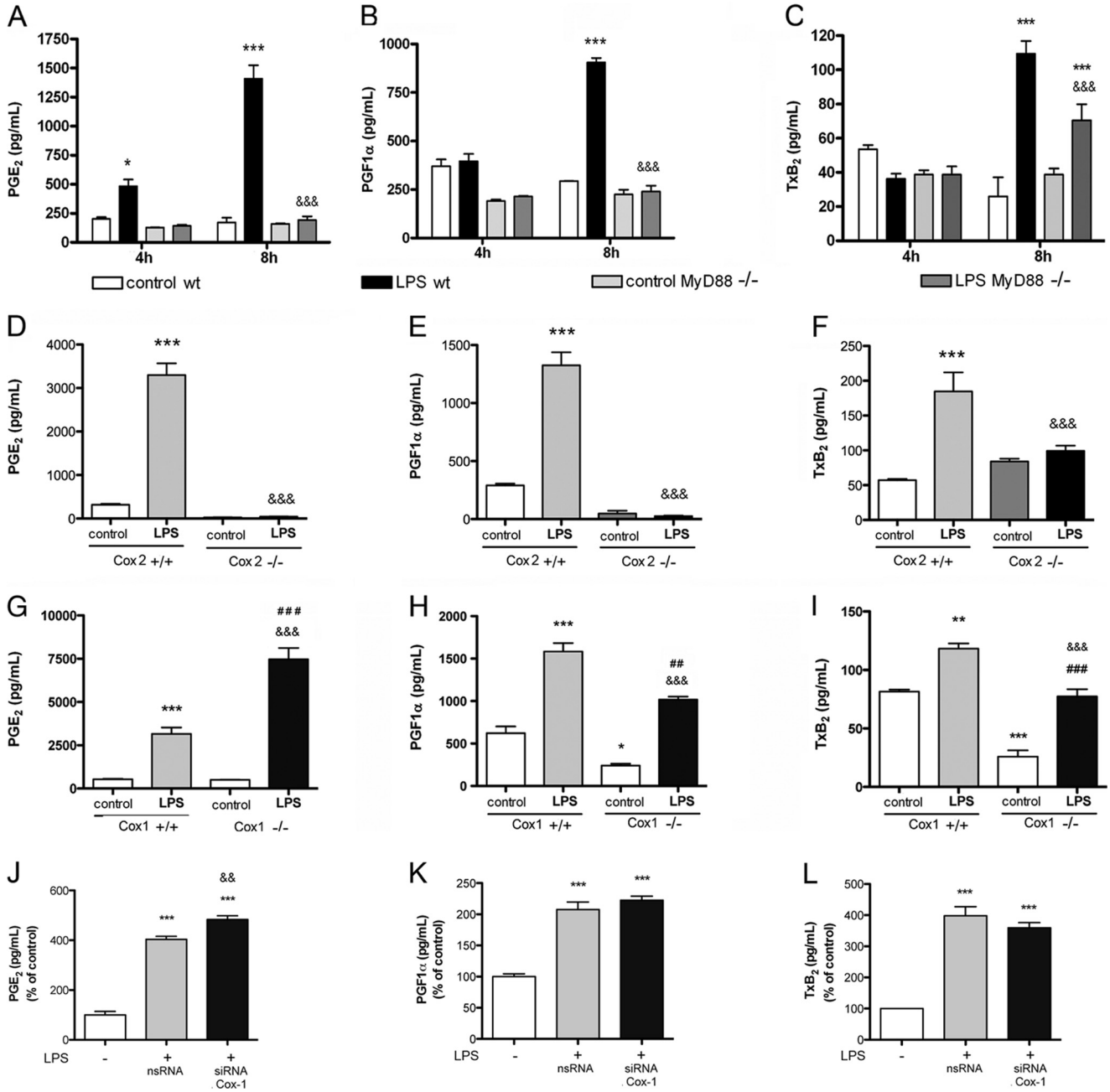

FIGURE 8. **LPS-induced prostanoid production is dependent on COX-2 although COX-1 exerts selective regulatory effects.** Purified cultures of mouse astrocytes were treated with LPS (10 ng/ml), and the concentration of prostanoids in the culture medium was studied by ELISA. Cells were collected at 4 and 8 h (*A–C*), or 8 h (*D–I*) after LPS. *A–C,* production of prostanoids is strongly attenuated in MyD88-deficient cells. *D–F,* LPS does not induce PGE_2 (*G*), PGF1α (*H*), or TxB_2 (*I*) in *Cox-2* KO cells (−/−). *G–I,* production of PGE_2 induced by LPS is enhanced in *Cox-1*-deficient astrocytes (−/−) (*G*). In contrast, the production of PGF1α (*H*) and TxB_2 (*I*), as indirect assessments of PG and TxA_2, respectively, is smaller in Cox-1 KO cells (−/−) compared with the wild type (+/+), both in the presence or absence of LPS. *J–L*, silencing COX-1 expression with siRNA slightly enhances the production of PGE_2 (*J*) but does not modify the production of PGI_2 (*K*) or TxA_2 (*L*). $n = 3$ in at least two independent experiments. *One symbol*, $p < 0.05$; *two symbols*, $p < 0.01$; *three symbols*, $p < 0.001$. * indicates comparison *versus* control. & indicates comparison *versus* LPS in WT or after treatment with nonsilencing (*ns*) RNA. # indicates comparison *versus* control KO cells.

In contrast to the increased expression of COX-2 and mPGES-1, the expression of COX-1 was down-regulated in astrocytes after TLR-4 activation. Reduced expression of COX-1, together with increased COX-2 expression, was previously found in the lungs and hearts of LPS-treated rats (39). In addition, we found that LPS down-regulated the expression of the *Ts* gene in astrocytes, suggesting some link in the control of the expression of *Cox-1* and *Ts*. Despite down-regulation of *Pgis* and *Ts* mRNA, LPS enhanced the production of PGI_2 and TxA_2 but to a lower extent than it increased PGE_2. This apparently contradictory effect (*i.e.* reduction of mRNA but increase in enzymatic products) could be due to the time delay needed for an effective reduction of protein content following decreases of constitutive mRNA expression. It is feasible that down-regulation of these genes limits the production of PGI_2 and TxA_2 in astrocytes, while favoring the production of PGE_2 because of up-regulation of mPGES-1. Under basal nonstimulated conditions, *Cox-2*-deficient astrocytes produced less PGI_2 and TxA_2

than the wild type cells, and COX-2-deficient astrocytes showed unaltered concentrations of these prostanoids, suggesting that COX-1 was involved in the basal production of PGI_2 and TxA_2. However, after LPS, the production of PGI_2 and TxA_2 increased in *Cox-1*-deficient cells but not in *Cox-2*-deficient cells, demonstrating that COX-2 was mainly responsible for their up-regulation after this challenge. Likewise, the production of PGE_2 after LPS was fully dependent on COX-2. However, *Cox-1*-deficient cells produced more PGE_2 after LPS than the corresponding WT cells, suggesting that COX-1 exerts some negative control on COX-2-dependent PGE_2 production after LPS.

Taken altogether, these results demonstrate the key role of COX-2 in prostanoid production after LPS in astrocytes and show that the production of PGE_2 also depends on down-regulation of *Cox-1* gene expression. Finally, these findings show that astrocytes respond to proinflammatory triggers with a strong generation of vasoactive PGE_2 that might exert effects on the adjacent brain microvasculature and contribute to modulate CBF responses to neuroinflammation.

Acknowledgments—We thank Francisca Ruiz and Eva Roig for excellent technical assistance.

REFERENCES

1. Hata, A. N., and Breyer, R. M. (2004) Pharmacology and signaling of prostaglandin receptors. Multiple roles in inflammation and immune modulation. *Pharmacol. Ther.* **103,** 147–166
2. Iadecola, C., Niwa, K., Nogawa, S., Zhao, X., Nagayama, M., Araki, E., Morham, S., and Ross, M. E. (2001) Reduced susceptibility to ischemic brain injury and *N*-methyl-D-aspartate-mediated neurotoxicity in cyclooxygenase-2-deficient mice. *Proc. Natl. Acad. Sci. U.S.A.* **98,** 1294–1299
3. Nagayama, M., Niwa, K., Nagayama, T., Ross, M. E., and Iadecola, C. (1999) The cyclooxygenase-2 inhibitor NS-398 ameliorates ischemic brain injury in wild-type mice but not in mice with deletion of the inducible nitric-oxide synthase gene. *J. Cereb. Blood Flow Metab.* **19,** 1213–1219
4. Araki, E., Forster, C., Dubinsky, J. M., Ross, M. E., and Iadecola, C. (2001) Cyclooxygenase-2 inhibitor ns-398 protects neuronal cultures from lipopolysaccharide-induced neurotoxicity. *Stroke* **32,** 2370–2375
5. Candelario-Jalil, E., González-Falcón, A., García-Cabrera, M., León, O. S., and Fiebich, B. L. (2007) Post-ischemic treatment with the cyclooxygenase-2 inhibitor nimesulide reduces blood-brain barrier disruption and leukocyte infiltration following transient focal cerebral ischemia in rats. *J. Neurochem.* **100,** 1108–1120
6. Candelario-Jalil, E., and Fiebich, B. L. (2008) Cyclooxygenase inhibition in ischemic brain injury. *Curr. Pharm. Des.* **14,** 1401–1418
7. Choi, J. K., Jenkins, B. G., Carreras, I., Kaymakcalan, S., Cormier, K., Kowall, N. W., and Dedeoglu, A. (2010) Anti-inflammatory treatment in AD mice protects against neuronal pathology. *Exp. Neurol.* **223,** 377–384
8. ADAPT Research Group, Lyketsos, C. G., Breitner, J. C., Green, R. C., Martin, B. K., Meinert, C., Piantadosi, S., and Sabbagh, M. (2007) Naproxen and celecoxib do not prevent AD in early results from a randomized controlled trial. *Neurology* **68,** 1800–1808
9. Aisen, P. S., Thal, L. J., Ferris, S. H., Assaid, C., Nessly, M. L., Giuliani, M. J., Lines, C. R., Norman, B. A., and Potter, W. Z. (2008) Rofecoxib in patients with mild cognitive impairment. Further analyses of data from a randomized, double-blind, trial. *Curr. Alzheimer Res.* **5,** 73–82
10. Grosser, T., Fries, S., and FitzGerald, G. A. (2006) Biological basis for the cardiovascular consequences of COX-2 inhibition. Therapeutic challenges and opportunities. *J. Clin. Invest.* **116,** 4–15
11. Aid, S., Langenbach, R., and Bosetti, F. (2008) Neuroinflammatory response to lipopolysaccharide is exacerbated in mice genetically deficient in cyclooxygenase-2. *J. Neuroinflammation* **5,** 17
12. Aid, S., Silva, A. C., Candelario-Jalil, E., Choi, S. H., Rosenberg, G. A., and Bosetti, F. (2010) Cyclooxygenase-1 and -2 differentially modulate lipopolysaccharide-induced blood-brain barrier disruption through matrix metalloproteinase activity. *J. Cereb. Blood Flow Metab.* **30,** 370–380
13. Choi, S. H., Langenbach, R., and Bosetti, F. (2008) Genetic deletion or pharmacological inhibition of cyclooxygenase-1 attenuate lipopolysaccharide-induced inflammatory response and brain injury. *FASEB J.* **22,** 1491–1501
14. Choi, S. H., Aid, S., and Bosetti, F. (2009) The distinct roles of cyclooxygenase-1 and -2 in neuroinflammation. Implications for translational research. *Trends Pharmacol. Sci.* **30,** 174–181
15. Choi, S. H., Aid, S., Choi, U., and Bosetti, F. (2010) Cyclooxygenases-1 and -2 differentially modulate leukocyte recruitment into the inflamed brain. *Pharmacogenomics J.* **10,** 448–457
16. Matsuura, T., Takuwa, H., Bakalova, R., Obata, T., and Kanno, I. (2009) Effect of cyclooxygenase-2 on the regulation of cerebral blood flow during neuronal activation in the rat. *Neurosci. Res.* **65,** 64–70
17. Ruiz-Valdepeñas, L., Martínez-Orgado, J. A., Benito, C., Millán, A., Tolón, R. M., and Romero, J. (2011) Cannabidiol reduces lipopolysaccharide-induced vascular changes and inflammation in the mouse brain. An intravital microscopy study. *J. Neuroinflammation* **8,** 5
18. Kunz, A., Park, L., Abe, T., Gallo, E. F., Anrather, J., Zhou, P., and Iadecola, C. (2007) Neurovascular protection by ischemic tolerance. Role of nitric oxide and reactive oxygen species. *J. Neurosci.* **27,** 7083–7093
19. Gordon, G. R., Mulligan, S. J., and MacVicar, B. A. (2007) Astrocyte control of the cerebrovasculature. *Glia* **55,** 1214–1221
20. Loftin, C. D., Trivedi, D. B., Tiano, H. F., Clark, J. A., Lee, C. A., Epstein, J. A., Morham, S. G., Breyer, M. D., Nguyen, M., Hawkins, B. M., Goulet, J. L., Smithies, O., Koller, B. H., and Langenbach, R. (2001) Failure of ductus arteriosus closure and remodeling in neonatal mice deficient in cyclooxygenase-1 and cyclooxygenase-2. *Proc. Natl. Acad. Sci. U.S.A.* **98,** 1059–1064
21. Gorina, R., Font-Nieves, M., Márquez-Kisinousky, L., Santalucia, T., and Planas, A. M. (2011) Astrocyte TLR4 activation induces a proinflammatory environment through the interplay between MyD88-dependent NFκB signaling, MAPK, and Jak1/Stat1 pathways. *Glia* **59,** 242–255
22. Paxinos, G., and Watson, C. (1986) *The Rat Brain in Stereotaxic Coordinates*, Academic Press, New York
23. Gorina, R., Santalucia, T., Petegnief, V., Ejarque-Ortiz, A., Saura, J., and Planas, A. M. (2009) Astrocytes are very sensitive to develop innate immune responses to lipid-carried short interfering RNA. *Glia* **57,** 93–107
24. Saura, J., Tusell, J. M., and Serratosa, J. (2003) High yield isolation of murine microglia by mild trypsinization. *Glia* **44,** 183–189
25. Friguls, B., Petegnief, V., Justicia, C., Pallàs, M., and Planas, A. M. (2002) Activation of ERK and Akt signaling in focal cerebral ischemia. Modulation by TGF-α and involvement of NMDA receptor. *Neurobiol. Dis.* **11,** 443–456
26. Livak, K. J., and Schmittgen, T. D. (2001) Analysis of relative gene expression data using real time quantitative PCR and the $2(-\Delta\Delta C(T))$ method. *Methods* **25,** 402–408
27. Wang, T., Qin, L., Liu, B., Liu, Y., Wilson, B., Eling, T. E., Langenbach, R., Taniura, S., and Hong, J. S. (2004) Role of reactive oxygen species in LPS-induced production of prostaglandin E_2 in microglia. *J. Neurochem.* **88,** 939–947
28. Guha, M., and Mackman, N. (2001) LPS induction of gene expression in human monocytes. *Cell. Signal.* **13,** 85–94
29. Lamon, B. D., Upmacis, R. K., Deeb, R. S., Koyuncu, H., and Hajjar, D. P. (2010) Inducible nitric-oxide synthase gene deletion exaggerates MAPK-mediated cyclooxygenase-2 induction by inflammatory stimuli. *Am. J. Physiol. Heart Circ. Physiol.* **299,** H613–H623
30. Smith, E. F., 3rd (1989) Thromboxane A_2 in cardiovascular and renal disorders. Is there a defined role for thromboxane receptor antagonists or thromboxane synthase inhibitors? *Eicosanoids* **2,** 199–212
31. Brenneis, C., Maier, T. J., Schmidt, R., Hofacker, A., Zulauf, L., Jakobsson, P. J., Scholich, K., and Geisslinger, G. (2006) Inhibition of prostaglandin E_2 synthesis by SC-560 is independent of cyclooxygenase 1 inhibition. *FASEB J.* **20,** 1352–1360

32. Ueno, N., Murakami, M., Tanioka, T., Fujimori, K., Tanabe, T., Urade, Y., and Kudo, I. (2001) Coupling between cyclooxygenase, terminal prostanoid synthase, and phospholipase A_2. *J. Biol. Chem.* **276,** 34918–34927
33. Johann, S., Kampmann, E., Denecke, B., Arnold, S., Kipp, M., Mey, J., and Beyer, C. (2008) Expression of enzymes involved in the prostanoid metabolism by cortical astrocytes after LPS-induced inflammation. *J. Mol. Neurosci.* **34,** 177–185
34. Díaz-Muñoz, M. D., Osma-García, I. C., Cacheiro-Llaguno, C., Fresno, M., and Iñiguez, M. A. (2010) Coordinated up-regulation of cyclooxygenase-2 and microsomal prostaglandin E synthase 1 transcription by nuclear factor κB and early growth response-1 in macrophages. *Cell. Signal.* **22,** 1427–1436
35. Ikeda-Matsuo, Y., Ikegaya, Y., Matsuki, N., Uematsu, S., Akira, S., and Sasaki, Y. (2005) Microglia-specific expression of microsomal prostaglandin E_2 synthase-1 contributes to lipopolysaccharide-induced prostaglandin E_2 production. *J. Neurochem.* **94,** 1546–1558
36. Chaudhry, U. A., Zhuang, H., Crain, B. J., and Doré, S. (2008) Elevated microsomal prostaglandin-E synthase-1 in Alzheimer disease. *Alzheimers Dement.* **4,** 6–13
37. Satoh, K., Nagano, Y., Shimomura, C., Suzuki, N., Saeki, Y., and Yokota, H. (2000) Expression of prostaglandin E synthase mRNA is induced in β-amyloid-treated rat astrocytes. *Neurosci. Lett.* **283,** 221–223
38. Wu, T., Wu, H., Wang, J., and Wang, J. (2011) Expression and cellular localization of cyclooxygenases and prostaglandin E synthases in the hemorrhagic brain. *J. Neuroinflammation* **8,** 22
39. Liu, S. F., Newton, R., Evans, T. W., and Barnes, P. J. (1996) Differential regulation of cyclo-oxygenase-1 and cyclo-oxygenase-2 gene expression by lipopolysaccharide treatment *in vivo* in the rat. *Clin. Sci.* **90,** 301–306